IEEE Access
Multidisciplinary | Rapid Review | Open Access Journal

Received January 27, 2022, accepted February 11, 2022, date of publication February 15, 2022, date of current version February 24, 2022.

Digital Object Identifier 10.1109/ACCESS.2022.3151868

A High-Accuracy and Fast Retrieval Method of Atmospheric Parameters Based on Genetic-BP

JIASHENG TIAN AND JIAN SHI

School of Electronic Information and Communications, Huazhong University of Science and Technology, Wuhan, Hubei 430074, China

Corresponding author: Jiasheng Tian (tianjs@hust.edu.cn)

This work was supported in part by the National Natural Science Founding of China under Grant 41876104 and Grant 41676090.

ABSTRACT In this article, we propose an accurate and fast method that is based on the genetic algorithm and the Back-Propagation neural network (GABP) to improve the accuracy and speed of retrieving atmospheric parameters (temperature, humidity, liquid water content, and so on). Firstly, the genetic algorithm is applied to improve and optimize the connection weights and thresholds of the BP neural network according to situ data measured by an sixteen-channel ground-based radiometer and a radiosonde, and then obtain a more proper range of those weights and thresholds. Secondly, the BP neural network is trained once again to get an ideal BP neural network model in a relatively short time. Finally, the model (or GABP), in which a genetic algorithm (GA) is combined with the BP neural network algorithm, is tested by the situ measurements of the sixteen-channel microwave radiometer. The tested results by GABP are not only in a good agreement with those of other known models, and but also has better accuracy and faster convergence speed than those reported algorithms for retrieving atmospheric parameters. It can make a conclusion that GABP is a new algorithm which is capable of quickly retrieving accurately atmospheric parameters.

INDEX TERMS Remote sensing of atmosphere, BP neural network, genetic algorithm, microwave radiometer.

I. INTRODUCTION

Generally speaking, a microwave radiometer can be applied to retrieve the atmospheric temperature, humidity, liquid water content, and other parameters [1], [2] based on its measured brightness temperature data. It is widely applied in such related areas as numerical weather forecasting and climate change research and so on. Firstly, it can be applied in the meteorological satellite to obtain atmospheric parameters. Secondly, it has important applications in atmospheric science research, for instance, forecasting the weather [3]. Finally, it can also provide data for relative corrections of the parameters measured by satellites or other measuring instruments, such as altimeters [4], [5]. A satellite altimeter measures the sea surface height (SSH) by the echo time of the rough sea surface [4], [6], [7]. The echo time is relative to the atmospheric dielectric constant and water vapor content; that is to say, a satellite radiometer can provide atmospheric corrections for a satellite altimeter with water vapor and liquid water contents [6]–[9].

The associate editor coordinating the review of this manuscript and approving it for publication was Stefania Bonafoni.

In recent decades, the ground-based microwave radiometer in atmospheric parameter detection has attracted more and more attention of many scholars and experts [10], [11]. The ground-based microwave radiometer has a higher accuracy for the detection of the lower tropospheric atmospheric parameters (less than 10km) than the spaceborne microwave radiometer [2], [12], [13], and also has the advantage of being less expensive for multiple channels detection [14]–[16] and the continuous observation of the local area [17], [18].

The ground-based microwave radiometer receives passive microwave signals of thermal radiation [19] from various altitudes in the atmosphere to obtain the atmospheric temperature, humidity, liquid water, and so on, based on relative retrieval methods. These retrieval methods are important and play a major role in obtaining atmospheric parameters with good accuracy and convergence speed [14], [15], [20].

Among those known retrieval methods, the linear regression [21] and the neural network [22], [23] are simple and easily applied to retrieve atmospheric parameters with acceptable accuracy. But they require a set of initial data [1], [24], for example, the neural network requires a set of prior data to be trained [25]–[27]. The iterative algorithm is also simple,

but its operating time is too long [1], [2]. The Kalman filter [28]–[30] is complex and rarely used. Some retrieval methods, such as optimization estimation, one-dimensional variational assimilation [31], [32], and the Bayesian maximum probability method [33], have to need estimate the prior profile and then compute the covariance from the prior data [2]. After decades of development, the BP neural network algorithm is widely used for retrieving atmospheric parameters and is becoming more suitable for atmospheric parameter retrieval. However, the network convergence speed of the BP neural network algorithm is a little slow due to the problem of finding the first derivative of the objective function. In general, for improving the convergence speed, there exists a kind of improved heuristic algorithms, such as the momentum Back Propagation [34], [35] and variable learning rate Back Propagation [36]. And also, there exists another kind of improved numerical optimization method, such as the conjugate gradient Back Propagation [37] and the Levenberg-Marquardt Back Propagation (LMBP) [38], [39]. Secondly, the BP neural network algorithm often gets trapped in local minima especially for non-linearly separable problems and can not find the actual global optimal solution due to the local convergence. There are several methods to improve the local convergence, such as the additional momentum method [40], [41], simulated annealing method [42], [43], and improved transfer function method, and so on. These improved algorithms have their own merits and demerits and have different effects in dealing with practical problems. To this day, local optimization still exists. When the BP neural network falls into the local optimal and minimum, it is incapable of jumping out of it. And thus, the retrieval time is so long that the accuracy is not so good. To resolve this problem, the genetic algorithm is introduced and combined with the BP neural network in this paper. The Genetic Algorithm–BP Neural Network Algorithm (GABP), which can find the optimal and minimum value from the global aspect, can also improve the accuracy and convergence speed of retrieving atmospheric parameters in a certain degree.

II. BP NEURAL NETWORK ALGORITHM AND GENETIC ALGORITHM

A. BP NEURAL NETWORK ALGORITHM

A general BP neural network is a multi-layer neural network [44], [45], whose structure is shown in Figure 1. $x_1, x_2, \ldots, x_M$ represent the input which is the brightness temperature measured by a radiometer, $y_1, \ldots, y_J$ represent the output which can be the atmospheric temperature from 0km to 10km height at a location. The model in Figure 1 can have several hidden layers, but only one input layer and one output layer. Each network layer consists of many neurons (sign ∘ in the hidden layer), by which the different network layers are connected with each other in terms of weights and thresholds. This connected design can allow the BP network to extract more efficient information from the input data and finish complex tasks of linearity or non-linearity [46].

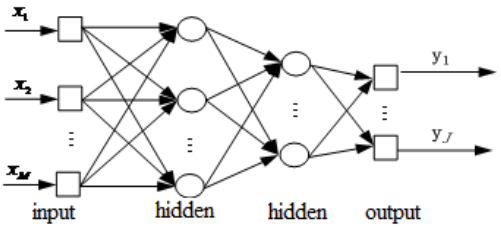

FIGURE 1. BP neural network structure.

To improve the accuracy and convergence speed, some improved BP network algorithms were presented in recent decades. For the standard BP network, those modified rules of the weights and thresholds are called the steepest descent method. Although those problems can be solved in a certain degree by this technology, there still exists a local minimum problem in addition to the slow convergence speed and the unstable network during training. To improve the standard BP neural network, several improved algorithms were proposed, which included an improvement of the learning algorithm and the determination of the network weights. The momentum BP algorithm introduced the momentum factor $\alpha(0 < \alpha < 1)$ [35], [40] in the corrected weighting $\Delta\omega(n)$ at the nth times as follows:

$$\Delta\omega(n) = -\eta(1-\alpha)\nabla e(n) + \alpha\Delta\omega(n-1) \tag{1}$$

where the second term $\alpha\Delta\omega(n-1)$ can make the weight ω update in a certain inertia, η is learning rate and $\nabla e(n)$ the gradient of the error at the nth times. However, updating the weight ω not only requires the gradient calculation but also the previous updated weight. The momentum BP algorithm has a certain ability of accelerating convergence and having an anti-oscillation, which makes it easier to find the minimum.

The learning rate variable BP algorithm [36], [40] has an adaptive ability of adjusting the learning rate gradient descent in terms of the variation of error. The learning rate will increase if the error decreases; otherwise, the adjustment is wrong, and the step size should be reduced.

The Newton BP method is a fast optimization algorithm based on the second order Taylor series expansion, but it is too complex to calculate the second derivative. To avoid the second derivative, an improved algorithm is proposed, which is called the quasi-Newton method [47]. The Levenberg Marquardt BP (LMBP) [37], [38] is an error-correcting algorithm which is designed to avoid the Hessian matrix calculations.

The BP neural network, as well as the other algorithms mentioned above, can be used to find out solutions of all kinds of complex objective functions. However, the excellent local optimization ability makes them fall easily in the local minimum if the function has multiple local minimum values because it is difficult to discover a global optimal solution among those local minimum values. In fact, the network weight training has always been caught in a local minimum from which it cannot jump out. On the other hand, the current

improvements do not involve an effective search for global optimization.

In this article, the improved BP network is based on the genetic algorithm and is good at finding global optimization, as well as improving the convergence speed and the accuracy for those retrieved parameters. The genetic algorithm can improve the BP neural network by optimizing: (1) the network connection weights and thresholds; (2) the network learning rules; and (3) the network structure. This article improves the BP neural network by optimizing the network connection weights and thresholds.

B. GENETIC ALGORITHM

The genetic algorithm is a method by which we can perform a global search for the optimal solution, based on Darwin's theory of evolution and Mendel's genetic theory. The genetic algorithm follows the principle of ''survival of the fittest''. In each of the generations of genetic inheritance, individuals who are more adaptable to the environment are selected, and then are used to have cross and mutation operations by the genetic rework method, resulting in a new approximate solution set.

The genetic algorithm includes individual coding, fitness evaluation, and genetic operation.

1) INDIVIDUAL CODING

The genetic algorithm encodes the parameters of the problem and transforms them into the coded individuals of the genetic space according to a certain structure so as to carry on the next step of genetic operation. Commonly, those encoding methods are binary code, floating-point coding, real coding, and so on. The coding by some real numbers is usually the primary consideration in most applications.

2) FITNESS EVALUATION

For the genetic algorithm, the fittest survives, and the unfit will be eliminated. Here, the magnitude of the fitness is determined by the fitness function, which is used to evaluate the current solution. The fitness function of a problem can be chosen as the function, itself, or its reciprocal. In general, the fitness function is easily calculated and can accurately find out the corresponding solution of those problems to be solved.

3) GENETIC OPERATION

In the genetic algorithm, there are three kinds of genetic operations: selection, crossover, and mutation.

The selection identifies those individuals who are more adaptable to the environment based on the fitness value.

Crossover is the most important operation in the genetic algorithm, mainly using some information of the parent population to generate new individuals through the cross operation. The design of the crossover operator is usually based on individual coding. If binary coding is used, single point, two points, and multi-point crossings can be selected.

Mutation can generate new individuals to sustain the diversity of the population. By combining the mutation and the selection, we can complete the global and local search of the solution space and avoid the loss of some effective information.

C. GENETIC ALGORITHM AND BP NEURAL NETWORK

The genetic algorithm is capable of finding out global optimization and is easily integrated with other technologies. Although the neural network has a strong non-linear mapping ability, it falls easily into the local minimum value. To avoid this problem, the genetic algorithm is introduced to improve the connection weights and thresholds of the BP neural networks.

This paper focuses on the initial connection weights and thresholds of the neural networks. The basic idea is to change the method of generating the initial weights of the network. The basic solution space of the decision variables (weights and thresholds) is estimated first, and then the optimal threshold value of the optimal network is selected by a genetic algorithm. The optimized values are substituted into the neural network for training according to:

$$\begin{cases} \min E(w, v, \theta, r) = \dfrac{1}{2}\displaystyle\sum_{k=1}^{N_1}\sum_{t=1}^{n}[y_k(t) - \hat{y}_k(t)]^2 \\ s, t : w \in R^{m\times p}, b \in R^{p\times n}, \theta \in R^p, r \in R^n \end{cases} \tag{2}$$

where $y_k(t)$ is the desired output, $\hat{y}_k(t)$ is the network output, E is the total error of the network. N is the number of sample sets, and N samples are divided into N_1 training samples and N_2 testing samples, respectively; m is the number of input nodes; p is the number of hidden nodes; n is the number of output nodes; w and θ represent the connection weight and threshold of the input layer-hidden layer corresponding to w and b shown in Figure 3, and v, r represents the connection weight and threshold of the hidden layer-output layer corresponding to w and b shown in Figure 3.

Supposing the transfer function is the sigmoid function f in the hidden layer, and the transfer function is a linear function for the output layer, the network output can be expressed by

$$\hat{y}_k(t) = \sum_{j=1}^{p} v_{jt} \cdot f[\sum_{i=1}^{m} w_{ij} \cdot x_i(t) + \theta_j] + r_t \tag{3}$$

where $x_i(t)$ is the value of the input layer. For GABP, it is required that the network total error E_1 should be less than ε_1, namely,

$$E_1 = E = \frac{1}{2}\sum_{k=1}^{N_1}\sum_{t=1}^{n}[y_k(t) - \hat{y}_k(t)]^2 \le \varepsilon_1 \tag{4}$$

and it is also necessary that the average mean square error E_2 is less than ε_2:

$$E_2 = \frac{1}{N - N_1}\sum_{k=N_1}^{N}\sum_{t=1}^{n}[y_k(t) - \hat{y}_k(t)]^2 \le \varepsilon_2 \tag{5}$$

where ε_1 and ε_2 are infinitesimal numbers according to the expected accuracy, respectively. In general, $E_1 < \varepsilon_1$ is to be

ensured, but $E_2 < \varepsilon_2$ is not necessarily to be considered in the BP network training. In this article, the genetic algorithm is used to find out the connected weights and thresholds of the global optimization by calculating the network error according to Equation (4) and (5). When Equation (4) and (5) hold, the output of the BP network will be reliable, and the model is established and can be used to retrieve atmospheric parameters.

For the sixteen-channel ground radiometer the genetic algorithm can be implemented in accordance with the following steps:

(1) Establish a three-layer BP network firstly and determine the initial solution space of weights and thresholds in terms of Equation (4) and (5). The neural network is established and trained, and then the network connection weights and thresholds are recorded. The maximum and minimum values of the network connection weights and thresholds are denoted as w_{max}/v_{max} and w_{min}/v_{min}, and $[w_{min}/v_{min}\text{-}\delta_1, w_{max}/v_{max} + \delta_2]$ is used as the basic solution space, where δ_1 and δ_2 are the adjustment constants.

(2) Determine the fitness function according to the neural network output error. Here the function is defined as:

$$F(w, v, \theta, r) = \frac{1}{\sqrt{\sum_{k=1}^{N_1}\sum_{t=1}^{n}[y_k(t) - \hat{y}_k(t)]^2}} \tag{6}$$

The greater the error, the smaller the fitness, so that Equation (6) can be represented by:

$$\begin{cases} \max F(w, v, \theta, r) \\ s, t : w \in R^{m\times p}, v \in R^{p\times n}, \theta \in R^{p}, r \in R^{n} \end{cases} \tag{7}$$

(3) Encode the basic solution space and determine the encoding length of genetic algorithm. If floating-point coding is used, the string length can be given as

$$L = m^*p + p^*n + p + n \tag{8}$$

where m^*p is the number of weights of the input-to-hidden layer, p^*n is the number of weights of the hidden-to-output layer, p is the number of thresholds of the hidden layer, and n is the number of thresholds of the output layer.

(4) Define the genetic algorithm parameters such as the population size, maximum number of iterations, crossover probability, and mutation probability, and then initialize the population pop according to the basic solution space given in step (1), which consists of M individuals.

(5) Calculate the individual's fitness. Each individual in population M is decoded to generate the corresponding network connection weights and thresholds. And the individual fitness is calculated according to Equation(6).

(6) The current population of the highest fitness of individuals is retained and does not participate in genetic operations, while other individuals will be going on to be chosen, crossed, and mutated.

(7) Generate a new generation of groups.

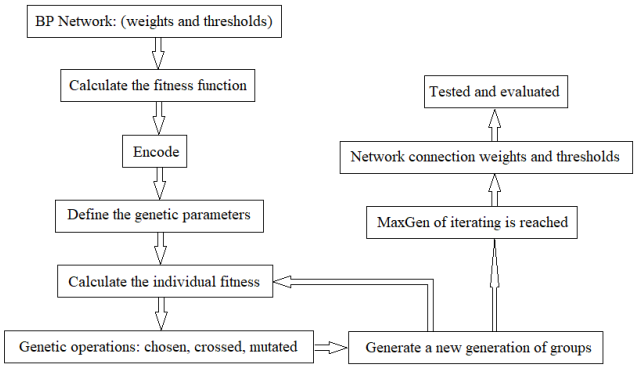

FIGURE 2. Steps of implementing genetic algorithm.

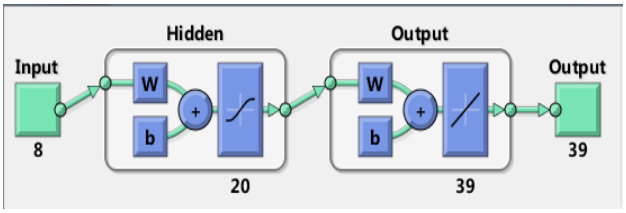

FIGURE 3. Atmospheric parameter inversion neural network structure shown by Matlab.

(8) Repeat step (5)∼(7) until the maximum number *MaxGen* of iterating is reached.

(9) Select those individuals with the highest adaptation in the first *MaxGen* generation and decode them to get the appropriate network connection weights and thresholds.

(10) Those connection weights and thresholds generated in step (9) are substituted into the network for training and testing, and then the network performance will be evaluated.

These steps can be explained as Figure 2.

III. ANALYSIS OF GABP RETRIEVING ATMOSPHERIC PARAMETERS

A. ANALYSIS OF GABP RETRIEVING ATMOSPHERIC TEMPERATURE

The atmospheric temperature vertical profile (or temperature profile) is a basic parameter in the atmospheric parameter inversion. In this section, the performance of GABP in retrieving atmospheric parameters is evaluated by comparing it with other methods in retrieving the atmospheric temperature. The GABP algorithm is compared with some other reported methods from these following aspects: the number of iterations, the training time, and the accuracy of retrieving. Those inversion methods include the steepest descent method, the momentum BP method, the learning rate variable BP method, the quasi-Newton method, and LMBP algorithm. The situ measurements are from the sixteen-channel radiometer detection and the probe balloon detection. The used network structure, which is shown by source codes of Matlab, is shown in Figure 3. In Figure 3, there are eight neurons in the input layer, 20 neurons in the hidden layer, and 39 neurons in the output layer. Eight neurons are defined by the number of the sixteen-channel radiometer (the eight-channel at V band and eight-channel at K band, and the total

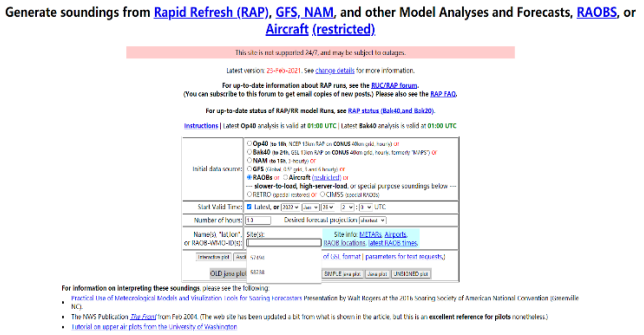

FIGURE 4. The situ data from the sounding data is loaded.

sixteen-channel). Thirty-nine neurons are the number of the temperature output points at 0∼10km height, as shown in the follows: 0, 10, 30, 50, 75, 100, 125, 150, 200, 250, 325, 400, 475, 550, 625, 700, 800, 900, 1000, 1150, 1300, 1450, 1600, 1800, 2000, 2200, 2500, 2800, 3100, 3500, 3900, 4400, 5000, 5600, 6200, 7000, 8000, 9000, 10000(m). In Figure 3 the brightness temperatures at 8-channel of V band or K band is regard as the input and temperatures measured by the sounding at 39 samples from 0 to 10km is regard as the output. After training the expected model is established, and then is tested by the testing data. To retrieve another atmospheric parameter needs to train and establish a model and then to test, an atmospheric parameter corresponds to a model.

Twenty neurons M in the hidden layer can be given by [48]

$$M = \sqrt{0.42nm + 0.12m^2 + 2.54n + 0.77m + 0.35} + 0.51 \tag{9}$$

where $m = 39$ is the number of neurons in the output layer, and $n = 8$ is the number of neurons in the input layer. W and b in Figure 3 stand for connection weights and thresholds, corresponding to w, θ, v, r in equation (3) respectively. For the input-hidden layer, W $= w$ and b $= \theta$ represent the connection weights and thresholds of the input layer-hidden layer. For the hidden-output, W $= v$ and b $= r$ represents the connection weights and thresholds of the hidden layer-output layer.

The situ data are from the sounding data, which can be obtained from http://rucsoundings.noaa.gov/ (time: 2011.1-2016.1, place: Wuhan city), as shown in Figure 4. In Figure 4 "57494" represents Wuhan and "58238" Nanjing.

From the situ data, the paper extracts pressure(pa), height(m), temperature profile, and dew point. Firstly, from the measurements of dew points corresponding to the pressure or height, the water vapor profile can be extracted. Secondly, by linear interpolation, we can obtain the temperature and water vapor profiles that meet the requirements. Finally, using the MPM93 model [49], the brightness temperature can be obtained. The next series of operations are neural network training, testing, and analysis. In these neural network algorithms, the evolution parameters of the network are the same values. The learning rate of the network is 0.01; the maximum number of iterations is defined as 500; the target error is 0.001, and the check value is 50 (the verification sample error is kept constant for 50 consecutive times, and then the training will end). The number of iterations, training time, and error are shown in Table 1. It is obvious from Table 1 that the test error of the steepest descent method(SD) is very large in the network training, and the network will no longer converge if the number of iterations reaches 187 times. The convergence effect of the momentum BP method(MBP) and the learning rate variable BP method(LRVBP) is higher than that of the steepest descent method(SD), and the number of iterations reaches 500. However, these testing errors are 2.32K and 3.73K, respectively, in the training of 500 iterations. These three methods still did not meet the requirements of retrieving atmosphere temperature, although the training time is only a few seconds. Their Gradients of error surface are large and the minimum is not obtained. The larger these gradients, the farther away from the minimum. The number of iterations for the quasi-Newton method(QN) is 266 times, and its testing error is 0.721K. The convergence of the quasi-Newton method(QN) is better, but its training time is obviously longer than those of LMBP algorithm and GABP algorithms, which affects the efficiency of network computing. LMBP and GABP are not very different in the number of iterations and training time, but both of them can converge rapidly in a short time. However, only the testing error of GABP is 0.00161, which is almost the same as the target setting error 0.001, while there is a big difference between the testing error and the target setting error for the other methods, such as SD, MBP and LRVBP.

TABLE 1. Comparison of several algorithms.

Algorithm	Number of iteration	Training time(s)	Testing error(K)	Gradient of error surface
SD	187	1	5.85	29
MBP	500	4	2.32	0.329
LRVBP	500	3	3.73	8.6
QN	266	138	0.721	0.682
LMBP	84	78	0.364	0.536
GABP	60	58	0.00161	0.00792

After analyzing the network training, it is necessary to use the test data to evaluate the performance of the neural network. In this paper, the root mean square error (*RMSE*) is used as:

$$RMSE = \sqrt{\frac{\sum_{i=1}^{N} (\hat{y}_i - y_i)^2}{N}} \tag{10}$$

where N is the number of test samples, $\hat{y}_i$ is the measured value of the sounding, and y_i is the network testing output.

RMSE of the temperature profile retrieved by these six algorithms(SD,MBP,LRVBP,QN,LMBP,GABP)are plotted in Figure 5. The data in Table 1 and Figure 5 shows that

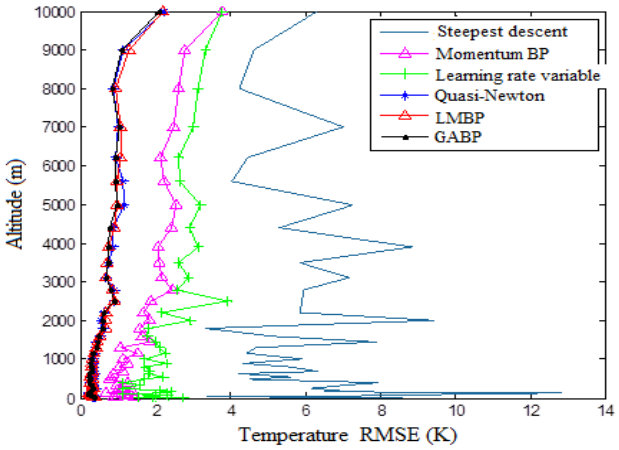

FIGURE 5. Temperature *RMSEs* of different algorithms.

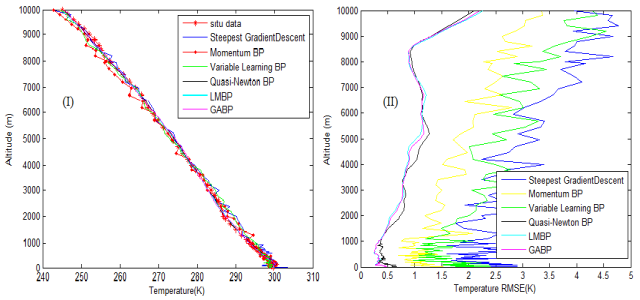

FIGURE 6. Temperature profiles and RMSE by several algorithms.

SD without any improvements has large oscillation and its convergence effect is also poor. To some degree, it does not converge. LRVBP or MBP method with some improvements can avoid network oscillation and improve network stability. The *RMSEs* of the temperature profiles retrieved by LRVBP and MBP fluctuate largely under 3000 or 2000 meters height, although the convergence effects of them are better. At the same time, the *RMSE*s of the retrieved results by LRVBP and MBP are still poor at more than 3000 meters. The *RMSEs* of QN, LMBP and GABP are almost the same, but the training time of QN is relatively longer. The performance of GABP is the same as that of LMBP, which is good and can be accepted in retrieving atmospheric parameters.

Similarly, another network is trained by 600 sets of samples and is tested by 297 sets of samples (time: 2010.1-2020.1, place: Wuhan city, 897 sets of samples). Temperature profiles retrieved by these six algorithms were shown in Figure 6(I). Firstly, SD, MBP and VRVBP spend several seconds for finishing the training, but their *RMSEs* are much larger than those of QN, LMBP and GABP, as shown in Figure 6(II). Secondly, they took longer using 897 sets of samples than 493 sets of samples, as shown in Figure 7. It is obvious that it takes longer and longer with the training data increasing, even more than several times longer especially for QN, LMBP and GABP with good accuracy.

But from Figure 7 it is obvious that the mean square error(*MSE*) of temperatures retrieved by QN, LMBP and GABP reduce slowly and almost keep constant in a certain

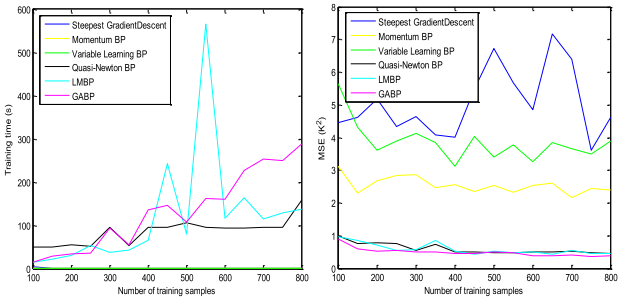

FIGURE 7. Training time(left) and retrieving accuracy(right) by several algorithms.

TABLE 2. Frequency channels of the based-ground radiometer.

Wave band	K band	V band	Band width
Frequency (GHz)	22.24	51.26	0.3
	23.04	52.28	0.3
	23.84	53.86	0.3
	25.44	54.94	0.3
	26.24	55.5	0.3
	27.84	56.66	0.3
	30	57.3	0.3
	31.4	58	0.3

degree when the number of training samples arrives at 400. The retrieving accuracy of these three algorithms is less than $1K^2$ and almost the same, and also training time can also be accepted when the number of training samples is 400. Although the retrieving accuracy become better and better with training samples increasing, as shown in Figure 7(right), but the training time becomes longer and longer with training samples increasing, as shown in Figure 7(left). Therefore, it is not necessary to increase training samples until 800 or more than in order to obtain a slightly good accuracy.

B. GABP RETRIEVING TEMPERATURE PROFILE

According to the sixteen-channel radiometer, the temperature profile is retrieved from the brightness temperature data of V band with eight channels, the water vapor, and liquid water content is retrieved from the brightness temperature data of K band with eight channels. Humidity can be retrieved from K band and V band, or be calculated by the retrieved temperature and water vapor. We use the different model for different parameters. The brightness temperature data of K-band and relative sounding data are used to train and establish GABP model of retrieving temperature profiles, and then the established model will be tested and evaluated. The brightness temperature data of V-band and the relative sounding data are used to train and establish GABP model of retrieving the water vapor, and liquid water content, respectively. And then the two models will be tested and evaluated. The center frequency and its band width of the sixteen-channel ground-based radiometer are shown in Table 2. The noise of the radiometer is 3dB and can be

FIGURE 8. The 16-channel radiometer(left) and its test site.

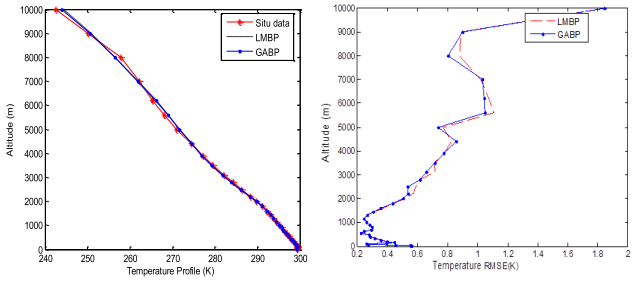

FIGURE 9. Temperature profile(left) and its *RMSE*(right).

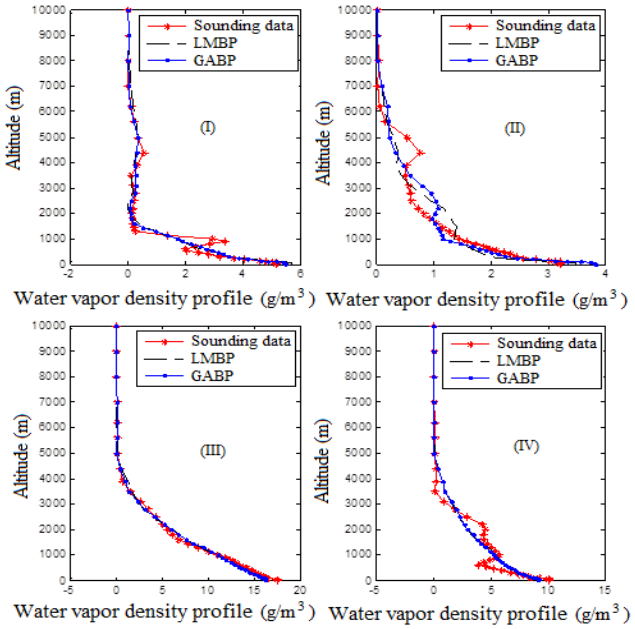

FIGURE 10. Comparison of water vapor density profile inversion and sounding data.

counterbalanced by the integral time with one second. The radiometer is equipped in Wuhan shown in Figure 8.

There are 400 groups of training samples and 93 groups of testing samples from the situ data in Wuhan city. The time of these situ data is from January 2011 to January 2016. Some clear days without clouds are chosen. The temperature profiles and *RMSEs* of LMBP and GABP are shown in Figure 9. Those curves in Figure 9 illustrate that *RMSEs* of the two algorithms is small and can be accepted. It can be found that the inversion error range of the two algorithms is from 0.23K to 2.22K in temperature profile inversion. But *RMSE* of GABP is smaller than LMBP at most points. Between LMBP and GABP, training time and testing time of GABP(164.3868s) are shorter than those of LMBP(257.5945s), and also the accuracy of GABP(mean(*RMSE*) = 0.5366K) is higher than that of LMBP(0.5469K). At 2km or less, the network output is consistent with the actual measurement results (or situ sounding data). The inversion error or *RMSE* of atmospheric temperature is below 1K. At the altitude of 2km ∼ 9km, *RMSE* varies from 1K to 1.5K, and these inversion results can be accepted and are ideal. In general, some parameters of the lower atmosphere measured by the radiometer are more accurate than those of the upper atmosphere. The temperature is an example. The radiation of the lower atmosphere is received directly by the radiometer, while the radiation of the upper atmosphere is received by the radiometer after it is attenuated during passing through the lower atmosphere. Thus, *RMSE* is larger at the altitude of 2km ∼ 9km than those at 2km or less.

C. GABP RETRIEVING WATER VAPOR PROFILE

The brightness temperature from a K-band 8-channel radiometer is used as the network input; the historical water vapor density from sounding balloon data is used as the network output. The network is trained by 400 sets of samples and is tested by 93 sets of samples. The tested results are shown in Figure 10(I-IV) and Figure 11, which are plotted by four sets of samples' results among those 93 sets of tested samples. To illustrate the results by GABP, four sets of testing samples are randomly chosen from these 93 sets of ones in Figure 10. In Figure 10 (I, III) the results by GABP and LMBP are almost consistent with the measured values(sounding data), although the retrieved results are quite different from sounding data at a few points, as shown in Figure 10 (II,IV). It is obvious that the retrieved water vapor profiles can be accepted in practices.

RMSE of the neural network based on LMBP algorithm is 0.082g/m^3 ∼ 1.115g/m^3, and *RMSE* based on GABP algorithm is 0.062g/m^3 to 0.921g/m^3. *RMSE* of the two algorithms at more than 6km is small because the water vapor density is small at more than 6km height, while *RMSE*s increase with the height decreasing because the contribution of water vapor density is large at low altitude. Obviously, GABP algorithm inversion accuracy is better, especially at a low altitude, the error is also relatively small in Figure 11(*a*). The relative error is less than 10% at low altitude, for example less than 2km in Figure 11(*b*). At most points (less than 8km height) the relative error is less than 40%, where the relative error is the retrieved *RMSE* divided by *RMSE* of Sounding data

D. GABP RETRIEVING RELATIVE ATMOSPHERIC HUMIDITY PROFILE

The relative atmospheric humidity profile can be directly obtained by using the 16-channel brightness temperature and

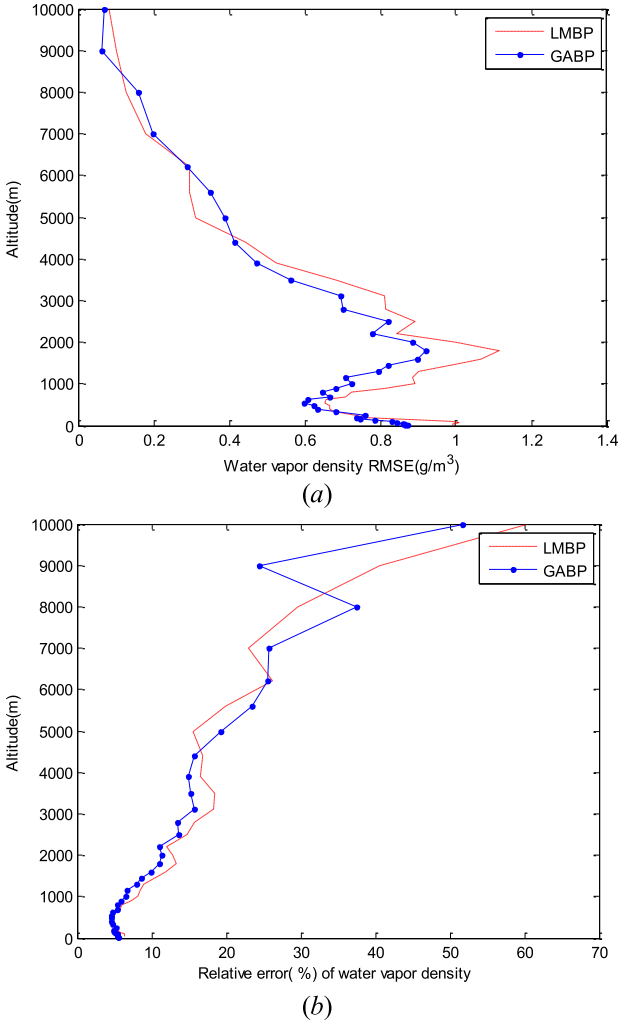

FIGURE 11. Comparison of inversion error RMSE (*a*) and Relative error (%) (*b*) of water vapor profile.

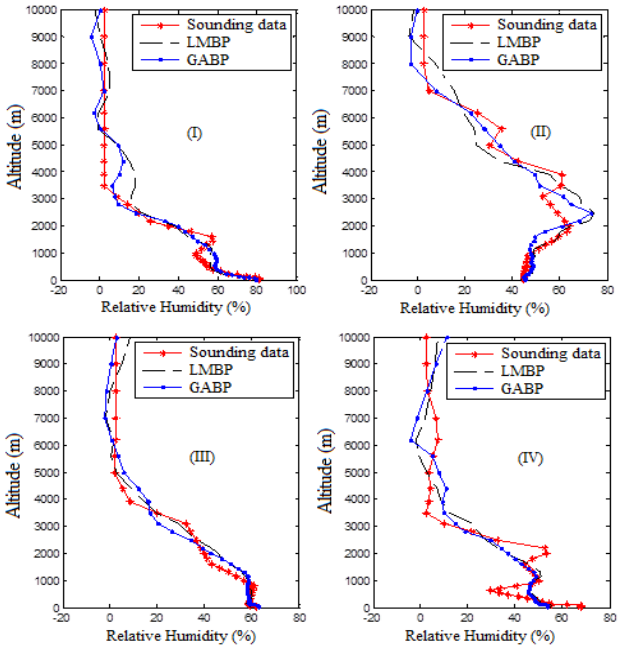

FIGURE 12. GABP and LMBP retrieving relative humidity profile and sounding data.

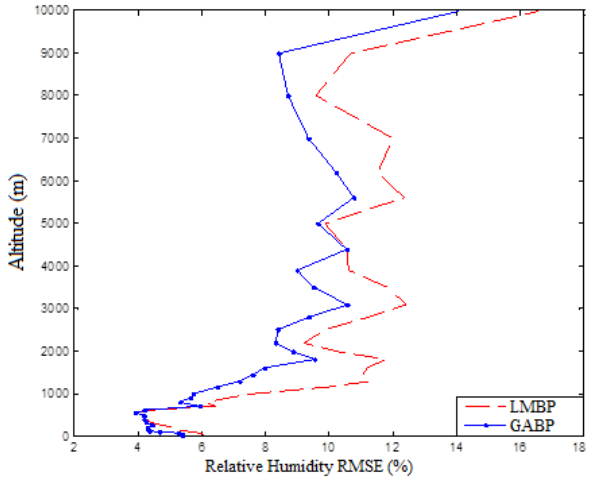

FIGURE 13. Comparison of relative humidity profile inversion.

also be derived from the temperature profile and water vapor density as the second method. In the article, the first method is chosen to establish a nonlinear relationship between the brightness temperature and the relative humidity through the neural network. The brightness temperature is used as the network input and the relative humidity as the network output, and then the network is trained to get a series of related network parameters, where the brightness temperature channels contain water vapor sensitive K-band and oxygen-sensitive V-band ones because the relative humidity is related to temperature and water vapor density.

The results estimated by LMBP and GABP are compared with the sounding values, as shown in Figure 12 (I-IV) and Figure 13. In Figure 12 four sets of testing samples are randomly chosen from these 93 sets of ones. Relative humidity decreases with altitude. However, at a few points relative humidity values retrieved by GABP or LMBP are negative. The reason for negative relative humidity values is that there exists a little abnormal data in the training samples, or the relative humidity is very low. For example the heavy raining, antennas Radome attached with water, radiometer calibration, or the very low relative humidity et al will give rise to negative relative humidity values. By processing these abnormal data and some corrections can solve the problem, or let the very low relative humidity (negative values) be zero. In Figure 13, *RMSE*s of the two algorithms are 4% $\sim$ 16.5% and increase with height. *RMSE*s of the two algorithms are almost the same under 1km, but the performance of the neural network retrieving the relative humidity based on the GABP algorithm is better than those based on the LMBP at 1km $\sim$ 10km, as shown in Figure 13. In Figure 13 relative humidity *RMSE* of GABP is smaller than those of LMBP at almost all points.

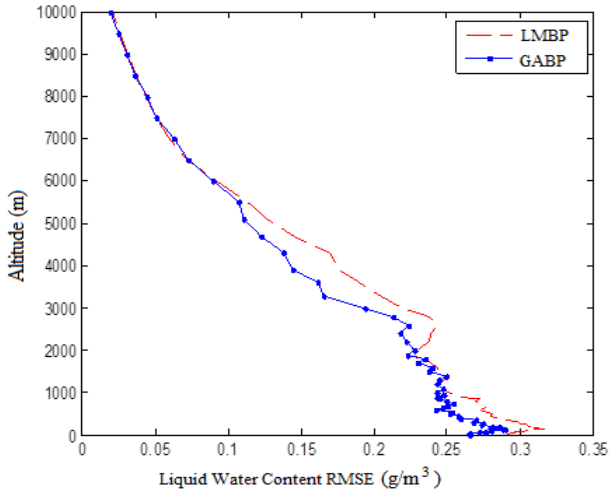

FIGURE 14. *RMSE*s of liquid water content by GABP and LMBP.

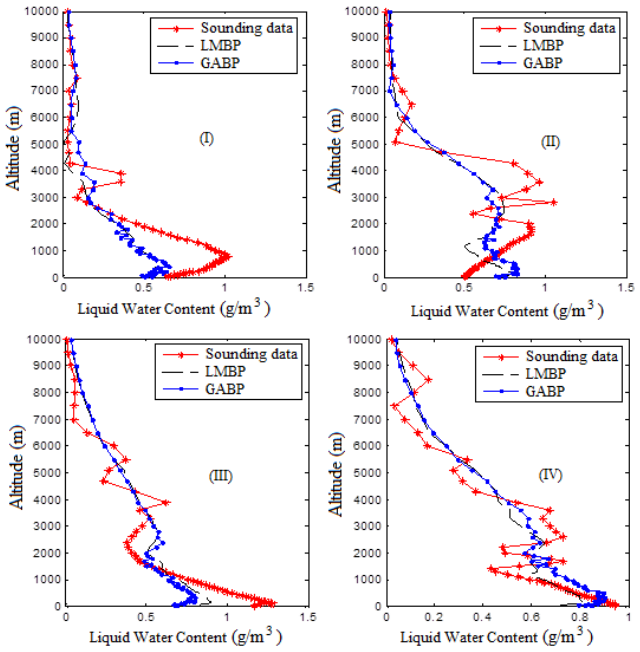

FIGURE 15. Results by GABP and LMBP and sounding data.

E. GABP RETRIEVING LIGUID WATER CONTENT

The liquid water content is 0 on a clear day without clouds and is not zero on a cloudy day with no rain, and the liquid water content mainly comes from the cloudy layer. The liquid water content is retrieved by the four channels with 22.24GHz, 23.04GHz, 23.84GHz and 31.4GHz of K band. 4 nodes in the input layer are chosen and 59 nodes in the output layer.

In the training of the network, 622 groups of cloudy data are divided into the training sample with 400 groups and the test sample data with 222 groups. The results retrieved by LMBP and GABP are shown in Figure 14 and Figure 15.

In Figure 14, *RMSE*s of liquid water content retrieved by GABP and LMBP decrease as the height increases, and is less than 0.1g/m^3 at more than 5km, and is 0.1g/m^3 $\sim$ 0.32g/m^3 below 5km. In Figure 15(I–IV), the four-random-testing

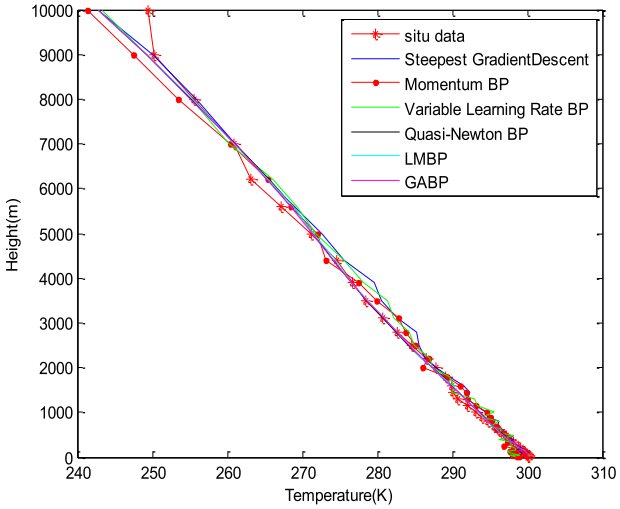

FIGURE 16. The temperature profile by several algorithms in Nanjing.

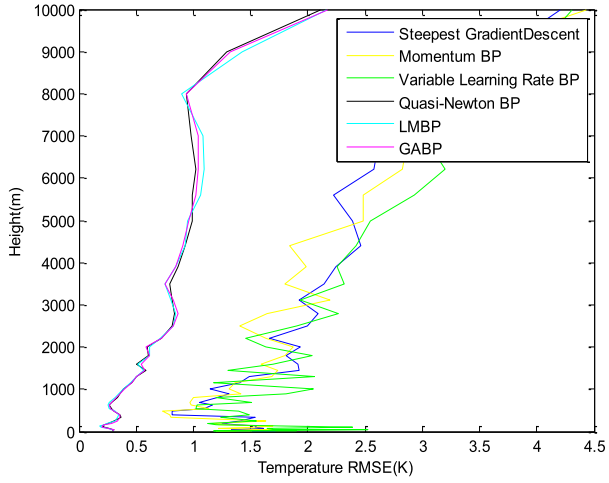

FIGURE 17. The temperature *RMSE* by several algorithms in Nanjing.

liquid water content profiles retrieved by GABP are almost the same as those by LMBP. However, results retrieved by GABP and LMBP are much different from the radiosonde data, especially below 5km, which is related to the variations of the sounding data itself at low altitudes. In other words, the accuracy of the measured samples in the lower layers is not the same as those in the upper layers because the liquid water content in the lower layers (below 5km) is larger and has a more complex variation than those in the upper layers.

F. GABP RETRIEVING ATMOSPHERIC PARAMETERS IN NANJING

In Figure 16, a temperature profile retrieved by SD, MBP, VLRBP, QN, LMBP and GABP in Nanjing city is shown in Figure 15. 622 sets of samples are chosen from January 2010 to December 2019 in Nanjing. Similarly, 400 sets of samples are training ones and 222 sets of samples are testing ones. It is obvious that the temperature profile is almost the same as that of Wuhan from Figure 16. The temperature

TABLE 3. The time and accuracy of the temperature retrieved by several algorithms in Nanjing.

Algorithm	Training time (s)	Mean(*RMSE*)(K)
SD	2.416	1.8208
MBP	3.2897	1.7361
LRVBP	3.1761	1.9920
QN	148.53	0.5889
LMBP	54.9373	0.5917
GABP	69.6006	0.5905

distribution law is similar to that of Wuhan. *RMSE*s of the temperature profile retrieved by GABP is approximate the smallest among these algorithms in Figure 17. The training time and the accuracy (mean(*RMSE*))are given in Table 3. Mean(*RMSE*) is the average *RMSE* for the 39 points at the altitude. In Table 3 the accuracy of the temperature profile retrieved by GABP is the same as that retrieved by QN, LMBP and is good and can be accepted. However, the training time of QN is longer than GABP and LMBP. All in all, It can make a conclusion that GABP is a new effective method of retrieving atmospheric parameters.

IV. CONCLUSION

The combination of the BP neural network and the genetic algorithm is called as GABP algorithm in the paper. GABP can improve the convergence speed and local optimization to a large extent. The performances of GABP in retrieving atmosphere parameters are compared with other network algorithms. The compared results show that the performance of GABP algorithm is better than that of LMBP algorithm and is also much better than the other inversion algorithms in terms of precision, convergence time, and the number of iterations. Finally, GABP algorithm is used to retrieve atmospheric parameters by using LMBP algorithm as a reference. In the case of retrieving the temperature profile, *RMSE* of GABP is below 2.3K, and is the same as that of LMBP algorithm. In the water vapor density profile inversion, the error is very small at higher altitudes, and the error is less than 1.2g/m^3 at lower altitudes, and the error of relative humidity is 4%∼16.5%. The inversion error of the liquid water content is less than 0.1g/m^3 at more than 5km height, and the error range is 0.1g/m^3 ∼ 0.32g/m^3 below 5km height, and the error decreases as the height increases. Finally, GABP is applied to retrieve the atmospheric temperature profile in Nanjing city, and its performance is compared with other algorithms and discussed. Similarly, its performance is good, as is the same as those in Wuhan. All in all, the training performance and test performance of GABP algorithm are obviously superior to those of other neural network algorithms and can be a new ideal algorithm for retrieving atmospheric parameters. However, the training time of GABP is sometimes slightly longer than that of LMBP when the number of samples increases. The training time of GABP will be studied in detail in the future.

REFERENCES

[1] F. Solheim, J. R. Godwin, E. R. Westwater, Y. Han, S. J. Keihm, K. Marsh, and R. Ware, "Radiometric profiling of temperature, water vapor and cloud liquid water using various inversion methods," *Radio Sci.*, vol. 33, no. 2, pp. 393–404, Mar. 1998.

[2] D. Cimini, T. J. Hewison, L. Martin, J. Güldner, C. Gaffard, and F. S. Marzano, "Temperature and humidity profile retrievals from ground-based microwave radiometers during TUC," *Meteorologische Zeitschrift*, vol. 15, no. 1, pp. 45–56, Feb. 2006.

[3] W. He, H. Chen, and J. Li, "Influence of assimilating ground-based microwave radiometer data into the WRF model on precipitation," *Atmos. Ocean. Sci. Lett.*, vol. 13, no. 2, pp. 107–112, Mar. 2020.

[4] G. Hayne, "Radar altimeter mean return waveforms from near-normal-incidence ocean surface scattering," *IEEE Trans. Antennas Propag.*, vol. AP-28, no. 5, pp. 687–692, Sep. 1980.

[5] C. S. Ruf, S. J. Keihm, B. Subramanya, and M. A. Janssen, "TOPEX/POSEIDON microwave radiometer performance and in-flight calibration," *J. Geophys. Res. Oceans*, vol. 99, no. C12, pp. 24915–24926, 1994.

[6] B. D. Tapley, J. B. Lundberg, and G. H. Born, "The SEASAT altimeter wet tropospheric range correction," *J. Geophys. Res. Atmos.*, vol. 87, no. C5, pp. 3213–3220, 1982.

[7] F. Monaldo, "Path length variations caused by atmospheric water vapor and their effects on the measurement of mesoscale ocean circulation features by a radar altimeter," *J. Geophys. Res. Oceans*, vol. 95, no. C3, pp. 2923–2932, 1990.

[8] R. G. Lipes, R. L. Bernstein, V. J. Cardone, K. B. Katsaros, E. G. Njoku, A. L. Riley, D. B. Ross, C. T. Swift, and F. J. Wentz, "Seasat scanning multichannel microwave radiometer: Results of the Gulf of Alaska workshop," *Science*, vol. 204, no. 4400, pp. 1415–1417, Jun. 1979.

[9] J. Sastamoinen, "Atmospheric correction for troposphere and stratosphere in radio ranging of satellites, in the use of artical satellites for geodesy," *Geophys. Monogr.*, vol. 15, pp. 247–251, Jan. 1972.

[10] B. Yan-song, C. Xi, and Q. Cheng, "0–10 km temperature and humidity profiles retrieval from ground-based microwave radiometer," *J. Tropical Meteorol.*, vol. 24, no. 2, pp. 243–252, Jun. 2018.

[11] E. Y. Biryukov and V. S. Kostsov, "The use of linear regression relations derived from model and experimental data for retrieval of the water content of clouds from ground-based microwave measurements," *Atmos. Ocean. Opt.*, vol. 32, no. 5, pp. 569–577, Sep. 2019, doi: 10.1134/S1024856019050051.

[12] E. R. Westwater, W. B. Sweezy, L. M. Mcmillin, and C. Dean, "Determination of atmospheric temperature profiles from a statistical combination of ground-based profiler and operational NOAA 6/7 satellite retrievals," *J. Climate Appl. Meteorol.*, vol. 23, no. 5, pp. 689–703, May 1984.

[13] E. R. Westwater, W. Zhenhui, N. C. Grody, and L. M. Mcmillin, "Remote sensing of temperature profiles from a combination of observations from the satellite-based microwave sounding unit and the ground-based profiler," *J. Atmos. Ocean. Technol.*, vol. 2, no. 2, pp. 97–109, Jun. 1985.

[14] L. Zhao, Y. Ma, G. Zhang, and L. Yang, "The principle and error analysis of microwave radiometer MP-3000A," *Desert Oasis Meteorol.*, vol. 3, no. 5, pp. 54–57, Oct. 2009.

[15] C. Gaffard and T. J. Hewison. (2003). *Radiometrics MP3000 Microwave Radiometer Trial Report, Observations/Development Technical Report TR26, Met Office*. National Meteorological Library. Exeter, U.K. [Online]. Available: https://tim.hewison.org/

[16] R. Ware, R. Carpenter, J. Güldner, J. Liljegren, T. Nehrkorn, F. Solheim, and F. Vandenberghe, "A multichannel radiometric profiler of temperature, humidity, and cloud liquid," *Radio Sci.*, vol. 38, no. 4, pp. 1–13, 2003.

[17] F. De Angelis, D. Cimini, U. Löhnert, O. Caumont, A. Haefele, B. Pospichal, P. Martinet, F. Navas-Guzmán, H. Klein-Baltink, J.-C. Dupont, and J. Hocking, "Long-term observations minus background monitoring of ground-based brightness temperatures from a microwave radiometer network," *Atmos. Meas. Techn.*, vol. 10, no. 10, pp. 3947–3961, Oct. 2017.

[18] V. S. Kostsov, "Retrieving cloudy atmosphere parameters from RPG-HATPRO radiometer data," *Izvestiya, Atmos. Ocean. Phys.*, vol. 51, no. 2, pp. 156–166, Mar. 2015.

[19] A. T. C. Chang and T. T. Wilheit, "Remote sensing of atmospheric water vapor, liquid water, and wind speed at the ocean surface by passive microwave techniques from the Nimbus 5 satellite," *Radio Sci.*, vol. 14, no. 5, pp. 793–802, Sep. 1979.

[20] J. L. Sánchez, R. Posada, E. García-Ortega, L. López, and J. L. Marcos, "A method to improve the accuracy of continuous measuring of vertical profiles of temperature and water vapor density by means of a ground-based microwave radiometer," *Atmos. Res.*, vol. 122, pp. 43–54, Mar. 2013.
[21] H. E. Fleming, *A Comparison of Linear Inversion Methods by Examination of the Duality Between Iterative and Inverse Matrix Methods in Inversion Methods in Atmospheric Remote Sounding*, A. Deepak, Ed. New York, NY, USA: Academic, 1997.
[22] J. H. Churnside, T. A. Stermitz, and J. A. Schroeder, "Temperature profiling with neural network inversion of microwave radiometer data," *J. Atmos. Ocean. Technol.*, vol. 11, no. 1, pp. 105–109, Feb. 1994.
[23] F. D. Frate and G. Schiavon, "A combined natural orthogonal functions/neural network technique for the radiometric estimation of atmospheric profiles," *Radio Sci.*, vol. 33, no. 2, pp. 405–410, Mar. 1998.
[24] J. Güldner and D. Spänkuch, "Remote sensing of the thermodynamic state of the atmospheric boundary layer by ground-based microwave radiometry," *J. Atmos. Ocean. Technol.*, vol. 18, no. 6, pp. 925–933, Jun. 2001.
[25] F. Del Frate and G. Schiavon, "A neural network algorithm for the retrieval of atmospheric profiles from radiometric data," *Proc. IEEE Int. Geosci. Remote Sens. Symp. (IGARSS)*, Apr. 1997, pp. 2097–2099, doi: 10.1109/IGARSS.1997.609238.1997.
[26] W. J. Blackwell, "A neural-network technique for the retrieval of atmospheric temperature and moisture profiles from high spectral resolution sounding data," *IEEE Trans. Geosci. Remote Sens.*, vol. 43, no. 11, pp. 2535–2546, Nov. 2005.
[27] W. J. Blackwell, "Neural network retrieval of atmospheric temperature and moisture profiles from cloud-cleared AIRS/AMSU radiances," in *Proc. IEEE Int. IEEE Int. IEEE Int. Geosci. Remote Sens. Symp. (IGARSS)*, Sep. 2004, pp. 2066–2069.
[28] P. Basili, P. Ciotti, and D. Solimini, "Inversion of ground-based radiometric data by Kalman filtering," *Radio Sci.*, vol. 16, no. 1, pp. 83–91, Jan. 1981.
[29] Y. Han, E. R. Westwater, and R. A. Ferrare, "Applications of Kalman filtering to derive water vapor profiles from Raman lidar and microwave radiometers," *J. Atmos. Ocean. Technol.*, vol. 14, no. 3, pp. 480–487, Jun. 1997.
[30] W. H. Ledsham and D. H. Staelin, "An extended Kalman-bucy filter for atmospheric temperature profile retrieval with a passive microwave sounder," *J. Appl. Meteorol.*, vol. 17, no. 7, pp. 1023–1033, Jul. 1978.
[31] J. Yang and Q. Min, "Retrieval of atmospheric profiles in the New York state mesonet using one-dimensional variational algorithm," *J. Geophys. Research: Atmos.*, vol. 123, no. 14, pp. 7563–7575, Jul. 2018.
[32] Q. Liu and F. Weng, "One-dimensional variational retrieval algorithm of temperature, water vapor, and cloud water profiles from advanced microwave sounding unit (AMSU)," *IEEE Trans. Geosci. Remote Sens.*, vol. 43, no. 5, pp. 1087–1095, Apr. 2005.
[33] F. S. Marzano, A. Mugnai, G. Panegrossi, N. Pierdicca, E. A. Smith, and J. Turk, "Bayesian estimation of precipitating cloud parameters from combined measurements of spaceborne microwave radiometer and radar," *IEEE Trans. Geosci. Remote Sens.*, vol. 37, no. 1, pp. 596–613, Jan. 1999, doi: 10.1109/36.739124.1999.
[34] V. V. Phansalkar and P. S. Sastry, "Analysis of the back-propagation algorithm with momentum," *IEEE Trans. Neural Netw.*, vol. 5, no. 3, pp. 505–506, May 1994.
[35] X. Zhang and Y. Gao, "Based on momentum method BP neural network in the target recognition research and application," *Proc. SPIE*, vol. 8193, Sep. 2011, pp. 717–723, doi: 10.1117/.12.900494,2011.
[36] S. Xie, C. Zhang, and X. Xiao, "Adaptive inverse induction machine control based on variable learning rate BP algorithm," in *Proc. IEEE Int. Conf. Automat. Logistics*, Aug. 2007, pp.2367-2372, doi: 10.1109/ICAL.2007.4338973.
[37] A. Y. Al Bayati, N. A. Sulaiman, and G. W. Sadiq, "A modified conjugate gradient formula for back propagation neural network algorithm," *J. Comput. Sci.*, vol. 5, no. 11, pp. 849–856, Nov. 2009.
[38] F. A. Fangjihu, "An application based on Levenberg-Marquardt Bayesian regulation algorithm in power plate," in *Proc. China Int. Conf. Electr. Distrib. (CICED)*, Tianjin, China, Dec. 2018, pp. 825–828, doi: 10.1109/CICED.2018.
[39] S. Mishra, R. Prusty, and P. K. Hota, "Analysis of Levenberg-Marquardt and scaled conjugate gradient training algorithms for artificial neural network-based LS and MMSE estimated channel equalizers," in *Proc. Int. Conf. Man Mach. Interfacing (MAMI)*, Bhubaneswar, India, Dec. 2015, pp. 1–7, doi: 10.1109/MAMI.2015.
[40] H. Shao and G. Zheng, "Convergence analysis of a back-propagation algorithm with adaptive momentum," *Neurocomputing*, vol. 74, no. 5, pp. 749–752, Feb. 2011.
[41] W. Lili, L. Hongbo, C. Feng, C. Deyun, and F. Qishuai, "Identification of flow regimes based on adaptive learning and additional momentum bp neural network," in *Proc. 6th Int. Conf. Instrum. Meas., Comput., Commun. Control (IMCCC)*, Harbin, China, vol. 29, Jul. 2016, pp. 574–578, doi: 10.1109/IMCCC.2016.29.
[42] V. Jayaraman and A. Ross, "A simulated annealing methodology to distribution network design and management," *Eur. J. Oper. Res.*, vol. 144, no. 3, pp. 629–645, Feb. 2003.
[43] J.-L. Liu, "Novel taguchi-simulated annealing method applied to airfoil and wing planform optimization," *J. Aircr.*, vol. 43, no. 1, pp. 102–109, Jan. 2006.
[44] E. H. Shiguemori, J. D. S. da Silva, H. F. de Campos Velho, and J. C. Carvalho, "A multilayer perceptron approach for the retrieval of vertical temperature profiles from satellite radiation data," in *Proc. IEEE Int. Joint Conf. Neural Netw.*, Jul. 2005, pp. 2689–2693.
[45] L. Shi, "Retrieval of atmospheric temperature profiles from AMSU—A measurement using a neural network approach," *J. Atmos. Ocean. Technol.*, vol. 18, no. 3, pp. 340–347, Mar. 2001.
[46] F. D. Frate and G. Schiavon, "Nonlinear principal component analysis for the radiometric inversion of atmospheric profiles by using neural networks," *IEEE Trans. Geosci. Remote Sens.*, vol. 37, no. 5, pp. 2335–2342, Sep. 1999.
[47] T. Ishikawa, Y. Tsukui, and M. Matsunami, "Optimization of electromagnetic devices using artificial neural network with quasi-Newton algorithm," *IEEE Trans. Magn.*, vol. 32, no. 3, pp. 1226–1229, May 1996, doi: 10.1109/20.497465.
[48] G. Daqi, "On structures of supervised linear basis function feedforward three-layered neural networks," *Chin. J. Comput.*, vol. 21, no. 1, pp. 80–86, Jan. 1998.
[49] H. J. Liebe, "MPM—An atmospheric millimeter-wave propagation model," *Int. J. Infr. Millim. Waves*, vol. 10, no. 6, pp. 631–650, Jun. 1989.

JIASHENG TIAN was born in Hubei, China, in 1970. He received the Ph.D. degree in electronic information and technology from the Huazhong University of Science and Technology, in 2002. He currently works with the School of Electronic Information and Communications. His research interests include electromagnetic field computation, microwave remote sensing of the atmosphere and ocean, particularly ocean surface winds and waves, and the interaction between radar signal and precipitation, as well as retrieving algorithms of some data measured by radiometer and altimeter.

JIAN SHI was born in Hubei, China, in 1960. He received the Ph.D. degree in electronic information and technology from the Huazhong University of Science and Technology, in 2001. He currently works with the School of Electronic Information and Communications. His research interests include network communication, microwave remote sensing of the atmosphere and ocean, particularly ocean surface winds and waves, as well as communication protocol and algorithms.